Björn Winkler* and Victor Milman

Density functional theory based calculations for high pressure research

Abstract: Density functional theory based calculations are commonly employed to complement experimental high pressure research. Here, a brief overview of the underlying theory and available codes is provided, followed by some applications. The influence of the choice of the exchange-correlation functional on predicted structural parameters and physical properties is discussed.

Keywords: density functional theory, exchange-correlation functional, high pressure, elastic coefficients, phase transitions, lattice dynamics

*Corresponding Author: **Björn Winkler,** Inst. f. Geowissenschaften, Altenhöferallee 1, 60438 Frankurt a. M., Germany,
e-mail: b.winkler@kristall.uni-frankfurt.de
Victor Milman: Accelrys, Science Park, 334, CB4 0WN Cambridge, UK

1 Introduction

Density functional theory-based atomistic model calculations are currently the most widely employed approaches to study structure-property relations of inorganic crystalline compounds. The underlying formalism was established by Hohenberg and Kohn (1964), who showed that the total energy of electrons moving in an external potential is a unique functional of the electron density. Hence, the ground state of the quantum mechanical system of electrons in a solid can be found by minimizing the total energy with respect to the electron density. A practical scheme for DFT calculations has then been proposed by Kohn and Sham (1965), where the so-called Kohn–Sham (KS) equations have to be solved self-consistently:

$$\left[-\frac{1}{2}\nabla^2 + V_{\text{ext}} + \int \frac{\rho(\boldsymbol{r}')}{|\boldsymbol{r}-\boldsymbol{r}'|}\,\mathrm{d}\boldsymbol{r}' + V_{xc}(\boldsymbol{r})\right]\psi_i(\boldsymbol{r}) = \varepsilon_i\psi_i(\boldsymbol{r}) \tag{1}$$

$$\rho(\boldsymbol{r}) = \sum_i^n \left|\psi_i(\boldsymbol{r})\right|^2 \tag{2}$$

$$V_{xc} = \frac{\delta E_{xc}[\rho(\boldsymbol{r})]}{\delta n(\boldsymbol{r})} \tag{3}$$

where atomic units, i.e. $\hbar = e = m_e = 4\pi\epsilon_0 = 1$ have been used, ρ in Eqs. (1) and (2) is the electron density, and V_{xc} is the exchange-correlation potential. The first term in Eq. (1) corresponds to the kinetic energy of the electrons, the second one describes the external potential they experience due to the nuclei, the third is the Hartree potential which describes the interaction of the i-th electron with the average electron density, while the last term contains all those interelectronic interactions which have not been included in the previous terms, thus making DFT exact. This last term in the Hamiltonian of Eq. (1), the exchange-correlation potential, can formally be written as the derivative of the exchange-correlation energy, which is a functional of the electron density (Eq. (3)). This term needs to be approximated (see below). In effect, the KS equations describe a system of n interacting electrons in an external potential by mapping this on a system of n noninteracting electrons in an effective potential. In most implementations the Born-Oppenheimer approximation is employed, which separates the dynamics of the electrons from that of the much heavier nuclei. The background of this theory and its very many applications have been described in numerous text books, e.g. (Parr and Yang, 1989; Kryachko and Ludena, 1990; Koch and Holthausen, 1999; Martin, 2008; Engel and Dreizler, 2011).

The success of this computational approach is based on two factors. Firstly, a significant number of codes with differing implementations of DFT have been developed, so that for a very broad range of scientific questions a reliable modeling tool is readily available. This is in contrast, for example, to force-field models, where computationally extremely efficient codes, such as GULP (Gale and Rohl, 2003), are also readily available, but where the development and testing of a specific description of interatomic interactions may take several months and the transferability of that description to a new problem is not guaranteed. Secondly, the computational effort required is, for most problems, moderate, so that a few days of cpu time on a moderately sized cluster are sufficient to solve a problem. Of course, there are numerous questions, such as large scale molecular dynamics simulations to understand melting which require extre-

mely powerful supercomputers, but the overwhelming number of studies is currently performed on clusters with no more than a few hundred cores.

Numerous DFT-based codes are available to reseachers. The codes can be most easily classified according to the basis set they employ. Often used "planewave" codes, such as ABINIT (Gonze et al., 2002), CASTEP (Milman et al., 2000; Segall et al., 2002; Clark et al., 2005), Quantum Espresso (Giannozzi et al., 2009), or VASP Kresse and Furthmüller, 1996), are computationally efficient as the states of the electrons in the ionic core are not explicitly computed, but instead pseudopotentials or the projector augmented wave (PAW) method (Blöchl, 1994) are employed. The pseudopotentials were introduced for solving scattering problems as far back as 1930s, but their use in solid state physics truly exploded from 1980s (Bachelet et al., 1982; Vanderbilt, 1990) when reliable computational solutions based on the density functional theory became available. Pseudopotentials are designed to reproduce electron scattering by atoms in such a way that only valence electrons become relevant. Pseudopotential approximation generates pseudo-wavefunctions and hence a pseudo electron density which mimics the all-electron result where it matters – between atoms, where chemical bonds are formed. This approximation is similar to the well-known frozen core approximation which assumes that core electrons are strongly bound to the nucleus and are unchanged by the formation of molecules or solids. It shoud be noted that the accuracy of pseudopotential based calculations does depend on the quality of the pseudopotential itself. Simulations of systems in high-pressure conditions have to be checked carefully in this respect since interatomic distances can get much shorter than at ambient conditions; hence it is often necessary to reflect this in the pseudopotential design (Pickard and Needs, 2011).

The codes listed above are mature and easy to use, and allow the computation of a very broad range of properties. For these codes, there are typically only a few parameters which control the convergence behavior (such as the so-called kinetic cut-off energy and the *k*-space sampling), and hence it is straightforward to ensure that the results are well-converged. Databases of pseudo-potentials or PAW parameters are available for all elements, or can be generated using programs like OPIUM (OPIUM, 2011). Other codes employ atomic-centered basis set, such as the LCAO-code CRYSTAL (Dovesi et al., 2005), DMol^3 (Delley, 2000), FHI-aims (Blum et al. 2009) or the order-N code SIESTA (Soler et al., 2002), which makes them computationally very efficient, but requires greater care and expertise to ensure numerical convergence. Still other codes, such as the "all electron" code WIEN2k (Schwarz et al., 2002), have more complex basis sets, which allow to achieve high numerical accuracy, but may lead to a restricted functionality, for example with respect to full geometry optimization of low symmetry compounds, for which the stress tensor is required. Some codes allow a fully relativistic treatment and incorporation of the effect of spin-orbit coupling, while others are restricted to a scalar relativistic description. While some codes allow to use clusters or 2-dimensional slabs, in the context of high pressure research all codes employ periodic boundary conditions, which implies the use of super-cells for structures which have defects or where there is no long-range translational periodicity.

As has been mentioned above, currently DFT calculations require the use of an approximate description of the exchange-correlation, *xc*, interaction. Most codes allow the user a choice of exchange-correlation functionals beyond the local density approximation, LDA. The shortcomings of the LDA are very well established. LDA binding energies sometimes predict an incorrect ground state structure, and usually result in "overbinding", i.e. consistently too small lattice parameters. LDA as well as other DFT approximations can severely underestimate electron band gaps. A later DFT development was generalized gradient approximation, GGA, of which several variants have been proposed, such as the PBE formulation (Perdew et al., 1996), revised version, RPBE, (Hammer et al., 1999), PBE version for solids, PBESOL, (Perdew et al., 2008) and the Wu-Cohen approximation, WC, (Wu and Cohen, 2006). GGA calculations are known to typically "underbind", i.e. the lattice constants are slightly too large and the band gaps are still underestimated, but GGA does give improved binding energies.

LDA and GGA represent only the rungs 1 and 2 on the so-called Jacob's ladder of exchange correlation functionals (Perdew and Schmidt, 2001). Further developments such as meta-GGA (Tao et al., 2003; Zhao and Truhlar, 2006) produce more accurate descriptions of thermochemistry and ground state structures. A slightly different evolution branch of exchange-correlation potentials resulted in the number of hybrid functionals that combine LDA or GGA description with Hartree-Fock level of theory. The main area of application of such popular hybrid functionals as B3LYP (Becke, 1993) or HSE (Heyd et al., 2003, 2006) is mostly in thermochemistry or in physics of semiconductors. These functionals are more accurate for such properties as reaction energies and electron band gaps which are fundamental for these types of applications. There is at the moment a relatively

Tab. 1: Comparison of structural parameters of stishovite from experiment (Baur and Khan, 1971) and DFT-based models. The difference between the models is the choice of the *xc*-functional. As is typically observed, the LDA leads to an overbinding, giving too small lattice parameters, while the GGA-PBE and RPBE underbinds. The PBESOL and WC *xc*-functionals reproduce the experimental data best.

	a [Å]	*c* [Å]	*V* [Å^3]	O(*x*)	*d*1(Si–O) [Å]	*d*2(Si–O) [Å]	*c*/*a*
exp. (Baur and Khan, 1971)	4.1790(4)	2.6649(4)	46.54	0.3062(13)	1.757	1.810	0.6377
LDA	4.1400	2.6505	45.43	0.3055	1.747	1.789	0.6402
GGA-PBE	4.2189	2.6779	47.66	0.3070	1.766	1.831	0.6347
RPBE	4.2565	2.6871	48.68	0.3077	1.773	1.853	0.6313
PBESOL	4.1780	2.6663	46.54	0.3060	1.758	1.808	0.6382
WC	4.1768	2.6669	46.53	0.3066	1.758	1.808	0.6385

small body of work where such advanced functionals would be applied for studies of lattice properties, especially at high pressure conditions. This situation may change as calculations with hybrid functionals become computationally less expensive; e.g., Ottonello et al. (2009) showed that B3LYP provides a rather accurate description of lattice parameters and elastic stiffness coefficients of stishovite.

However, as the level of sophistication increases the computations become more demanding in terms of computing resources.

A comparison of lattice parameters, atomic coordinates and interatomic distances obtained with different exchange-correlation functionals for stishovite is given in Table 1.

This comparison shows the typical relation between structural parameters and *xc*-functional, i.e. the LDA gives too short lattice parameters and interatomic distances, while the GGA in the PBE or RPBE form yields too large values. The results obtained with PBESOL and WC *xc*-functionals are in very good agreement with the experimental data.

In order to overcome the failure of DFT-LDA/GGA calculations to correctly reproduce the insulating ground-state of transition metal oxides, extensions such as a "Hubbard U" (Anisimov et al., 1991; Dudarev et al., 1998; Cococcioni and de Gironcoli, 2005), which adds an on-site Coulomb repulsion for the 3*d*-or *f*-electrons, have been introduced. Other "post-GGA" approaches include already mentioned hybrid functionals, such as B3LYP (Becke, 1993), "screened exchange" (Seidl et al., 1996; Clark and Robertson, 2010), "self interaction correction" (Perdew and Zunger, 1981), addition of a semi-empirical dispersion term (Grimme, 2006; Grimme et al., 2010; Jurecka et al., 2007) and many others. The development of improved *xc*-functionals is a very active area of research.

2 Applications

Extensive reviews of DFT-based model calculations for high pressure research in the Earth Sciences have been given by Gillan et al. (2006), Wentzcovitch et al. (2010a), and Wentzcovitch et al. (2010b). Here, some general aspects and some recent developments will be described.

2.1 Structures at high pressures

In a typical calculation the ground state structure of a compound is obtained in the athermal limit (i.e. neglecting zero point motion) and at 0 GPa by minimizing the total energy with respect to the positions of the atoms and the lattice parameters. This is called a "full geometry optimisation". For cubic structures, where all atoms are located on special Wyckoff positions without any degree of freedom, this reduces to the computation of the volume-dependence of the total energy. A typical example of a high pressure study of a high symmetry compound is the computation of the behaviour of Ta up to 200 GPa (Söderling and Moriarty, 1998). This study compared fully relativistic and scalar relativistic models and derived equation of states from energy-volume curves. For the hypothetical hcp phase, Söderlind and Moriarty (1998) fixed the c/a-ratio. Today, most codes, with the exception of some which employ a complex basis set, provide the option to simultaneously optimize the lattice parameters and the internal coordinates, and hence it is now straightforward to obtain the total energy of force- and stress-free low symmetry compounds.

The computation of structures at high pressure (but still in the athermal limit) is then based on minimizing the enthalpy with respect to a non-zero stress tensor. There are numerous studies comparing experimentally determined pressure-induced changes of lattice parameters to theoretical data. Usually, equations of state are

fitted to the P–V data in order to conveniently describe the high pressure behaviour (Holzapfel, 2001), or, for those codes which do not permit the calculation of the enthalpy, the corresponding energy-volume relations are employed. The most popular isothermal equations of state are currently probably the 2nd and 3rd-order Birch-Murnaghan equations of state. Typically, there is an overestimation of the bulk modulus in LDA calculations and an underestimation of the bulk modulus in GGA calculations, but generally DFT calculations predict the experimentally observed lattice compression within a few percent. For example, in a comparative study Dewaele et al. (2004) found that GGA-calculations including spin-orbit coupling reproduced experimentally determined equation of state parameters of Ta, W, Cu and Al to within 2.5% for the ambient pressure volume, bulk modulus and pressure derivative of the bulk modulus for a pressure range up to 100 GPa.

There are still comparatively few experimental structure refinements of low symmetry compounds at high pressures, and hence there are few detailed comparisons of pressure-induced changes of structural parameters of low symmetry compounds. However, in those cases were a detailed comparison has been made, such as in the investigation of the pressure-dependence of the stereochemical activity of lone electron pairs in $Bi_2Ga_4O_9$ (Friedrich et al., 2010), the agreement is generally very good, with deviations of typically less than a few percent. DFT-models provide, however, more insight than is currently available from single crystal high pressure studies. In the study mentioned above, Friedrich et al. (2010) analyzed the theoretical electron density distribution, which is, due to the restricted access to reciprocal space in DAC based studies, not available in any detail experimentally. Also, there is still no experimental X-ray diffraction study in which the position of hydrogen atoms in a low-symmetry compound have been determined at high pressures, while it is well established that hydrogen positions are well reproduced by DFT calculations (Milman and Winkler, 2001). For example, in a recent study, Alvaro et al. (2012) presented a diffraction study of the pressure dependence of atomic positions in zoisite, but were unable to determine the hydrogen positions. A prior DFT-based study (Winkler et al., 2008a) had predicted the pressure-induced structural changes of zoisite and had also analysed the change in the lattice dynamics. The theoretical study correctly predicted the axial compressibilities, where the *a*-axis is significantly less compressible than the *b*-axis, which, in turn is less compressible than the *c*-axis, and also correctly predicted the decrease of the $d(O–H\cdots O)$ distance from 2.78 Å at ambient pressure to 2.6 Å at 10 GPa. In addition, the theoretical study (Winkler et al., 2008a) gave the positions of the hydrogen atom and correctly reproduced the pressure-induced changes in the IR spectrum.

In summary, in those cases where the supercell approach provides a reasonable description of the structure, the compression behavior at ambient or low temperatures will be reliably modelled by DFT-calculations. Structures in which Wyckoff positions are partially occupied, or where there is dynamic disorder, often cannot be satisfactorily described and will give an incorrect compression behaviour. A conventional GGA/LDA calculation will not work reliably for structures in which strong electronic correlation influences the compression behavior.

There are several methods to incorporate the effect of temperature in the model calculations, all of which require significant computational resources. The quasi-harmonic approximation, in which phonons don't interact with each other, but where the phonon frequencies depend on the volume, provides an expression for the free energy of crystalline solids. The theory of the QHA and many examples have been reviewed by Baroni et al. (2010) and Wentzcovitch et al. (2010a). The QHA allows us to compute thermal expansion coefficients and also the difference between the heat capacity at constant volume and at constant pressure, but cannot be used to study melts at high pressures and temperatures.

An alternative approach to QHA that produces properties beyond the harmonic approximation is molecular dynamics simulations. Conceptually, DFT-based molecular dynamics are the same as MD simulations based on forcefields, in that for a given configuration forces acting on the atoms are computed, the atom positions are then updated according to the chosen time-step, and this process is repeated over and over again. However, while force field-based calculations with ensembles of many thousand atoms (and nowadays millions of atoms) have been technically feasible for a long time (e.g., Winkler and Dove (1992)) DFT-based MD simulations are typically still limited to a few hundred atoms, as larger ensembles require enormous computational resources. However, some properties, like thermal expansion coefficients, can be obtained from very small ensembles (Milman et al., 2005).

2.2 Pressure-induced structural phase transitions

For those calculations where the energies are computed as a function of the unit cell volume, phase transitions

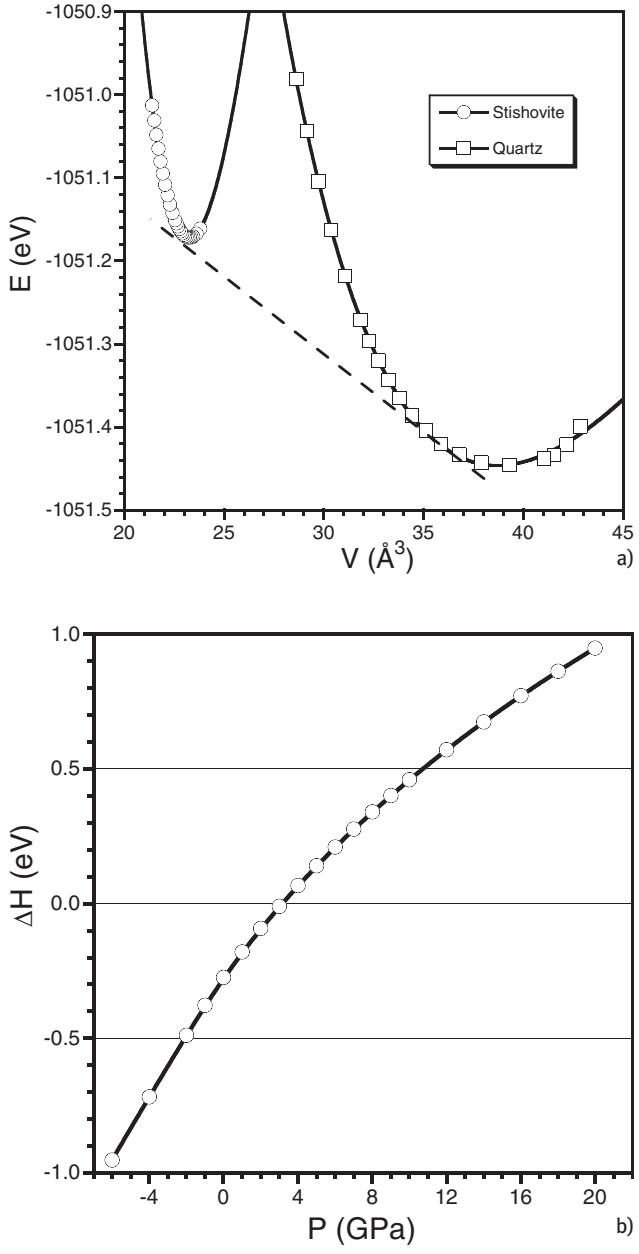

Fig. 1: Phase transition between two silica polytypes, α-quartz and stishovite. The common tangent construction is illustrated in the energy vs volume curve, while the enthalpy vs volume curve provides an easier way to determine the transition pressure.

can be obtained from the "common tangent" construction, where the slope of a tangent common to two E(V) curves gives the transition pressure (e.g. Winkler et al. (2000)). An example of such construction is shown in Fig. 1 where the energy-volume curves are calculated for silica polytypes, stishovite and α-quartz. Calculations were carried out with the WC *xc*-functional, and the points were obtained from geometry optimization calculations at fixed values of external pressure. The transition pressure can be calculated as the slope of the tangent in the E–V curve, although it is more convenient to compare enthalpies, $H = E + PV$. The plot of the enthalpy difference allows one to identify the transition pressure rather more easily. The two charts are complementary since the energy-volume curve provides additional information about the volume change associated with the transition.

It is not always straightforward to compare experimental and theoretical transition pressures. Most modelling studies predicting pressure-induced phase transitions are restricted to the athermal limit, and hence neglect the influence of temperature. In many experiments, the samples are compressed at ambient temperature, and hence reconstructive structural phase transitions may be kinetically hindered. The only way to demonstrate the absence of kinetic hindrance is to cross the phase boundary from both sides, but there are only few properly bracketed in situ studies of phase transitions in the diamond anvil cell. The use of non-hydrostatic pressure media may lead to pressure-induced amorphization, or lead to a significant lowering of the transition pressure (e.g. Bayarjargal et al. (2012)).

In a bracketed study of the pressure-induced B1–B2 transition of NaCl, Li and Jeanloz (1987) reported an ambient temperature transition pressure of 26.8 GPa, and a 0 K transition pressure of 28.2 GPa. The influence of the *xc*-correlation functional on the computed transition pressure was first investigated by Chall et al. (2000), where it was found that the LDA gave a transition pressure of 24.0 GPa, while the GGA-PBE gave a transition pressure of 24.6 GPa. A deviation between experimentally determined and theoretical transition pressures of a few GPa is typical for high pressured DFT-based model calculations.

A major recent achievement demonstrating the capabilities of DFT models was the computation of the high pressure/high temperature phase diagram of the α-, β-, and γ-phases in the system Mg_2SiO_4–Fe_2SiO_4, where LDA+"self-consistent"-U calculations were combined with the QHA and the virtual crystal approximation to obtain the relatively complex phase diagram of geophysically important transition metal containing solid solutions (Yu et al., 2013). However, the computational effort required for this study was significant.

An example where both experiment and theory have not yet come to an unambiguous conclusion is the case of pressure-induced changes in Cr_2O_3, which crystallizes in the corundum structure type at ambient conditions. The antiferromagnetic phase transition in Cr_2O_3 at $\approx$308 K at ambient pressure has attracted significant attention for a long time (Greenwald, 1951; Volger, 1952). However,

there is an open controversy with respect to the pressure dependence of the Néel temperature, dT_N/dP, where from neutron diffraction $dT_N/dP = -16(3)$ K/GPa (Worlton et al., 1968), while another experimental study found $dT_N/dP = +15.0(5)$ K/GPa from magnetoelectric susceptibility measurements (Gorodetsky et al., 1973). Recently, second harmonic measurements indicated that $dT_N/dP = -1.0(5)$ K/GPa and that this slightly negative pressure dependence of the Néel temperature leads to a magnetic phase transition at around 10 GPa (Bayarjargal and Winkler, 2013). Recent X-ray diffraction experimental single crystal structure determinations at pressures up to 55 GPa and at ambient temperature have unambiguously shown that there is no pressure-induced structural phase transition (Dera et al., 2011) and hence it seems that earlier findings of a pressure-induced structural phase transformation around 10–15 GPa during compression at ambient temperature were either due to non-hydrostatic conditions or due to a misinterpretation of Raman measurements (Bayarjargal and Winkler, 2013). Laser-heating experiments, however, have indicated a reconstructive phase transition at 30 GPa, but the structure of the new compound remained unsolved (Shim et al., 2004). DFT-models have not helped clarifying the situation up to now. Dobin et al. (2000) predicted a phase transition of Cr_2O_3 into a Rh_2O_3 (II) structure at 15 GPa, but didn't investigate a pressure-induced change in the magnetic structure of Cr_2O_3. Similarly, Wessel and Dronskowski (2013) predicted a phase transition of Cr_2O_3 into a Rh_2O_3 (II) structure at ≈14 GPa, but also seem not to have considered the possibility of a pressure-induced change in the magnetic structure. The benchmark, which would reliably confirm whether or not a structural model is correct, would be the reproduction of the Raman spectrum of the unknown high pressure phase recorded at 37 GPa by Shim et al. (2004).

2.3 Elasticity

A detailed comparison of experimentally determined and computed elastic stiffness coefficients of high pressure minerals has been given by Karki et al. (2001). The commonly used approach to obtain elastic stiffness coefficients is from stress-strain relations. There is a variety of tools available for automated calculations of elastic stiffness coefficients, e.g. (Perger et al., 2009; Golesorkhtabar et al., 2013; Accelrys, 2013).

The accuracy of DFT-based model calculations is about 5% for the diagonal coefficients, and about 10% for the off-diagonal coefficients. The choice of the *xc*-functional influences the results significantly, where the LDA gives an upper bound to the elastic stiffness coefficients, while the GGA-PBE provides a lower bound. An extensive comparison of elastic stiffness coefficients computed with LDA, GGA-PBE, PBESOL and WC-*xc* functionals (Milman, in prep.) has shown that the latter two outperform the first two approximations and this is also obvious from a comparison of the elastic stiffness coefficients of stishovite in Table 2.

Representation surfaces of the longitudinal elasticity (for a definition see Arbeck et al. (2012)) are given in Fig. 2.

Tab. 2: Elastic stiffness coefficients c_{ij} of stishovite. The first four data sets have been determined experimentally from Brillouin light scattering (Weidner et al., 1982; Brazhkin et al., 2005; Jiang et al., 2009) and from high frequency ultrasound resonance spectroscopy (Yoneda et al., 2012). Bosak et al. (2009) employed inelastic X-ray scattering data to rescale DFT-GGA results. The DFT-based data with different *xc*-functionals confirm the often made observations that LDA gives an upper bound for the tensor components, GGA-PBE or RPBE a lower bound and that the results of PBESOL and WC-based calculations are in between the two extremes.

	c_{11}	c_{33}	c_{12}	c_{13}	c_{44}	c_{66}
Weidner et al. (1982)	453(4)	776(5)	211(5)	203(4)	252(2)	302(3)
Brazhkin et al. (2005)	466(3)	775(4)	207(8)	204(4)	258(2)	310(6)
Jiang et al. (2009)	455(1)	762(1)	199(2)	192(1)	258(1)	321(1)
Yoneda et al. (2012)	443(3)	781(4)	193(2)	199(2)	256(2)	316(2)
exp. average	454(6)	774(8)	203(9)	200(6)	256(4)	312(7)
Bosak et al. (2009)	441(4)	779(2)	166(3)	195(1)	256(1)	319(1)
LDA	486(8)	756(2)	203(8)	193(1)	261(1)	329(1)
GGA-PBE	403(2)	699(3)	153(3)	176(1)	234(1)	288(1)
WC	438(3)	725(3)	188(3)	185(1)	246(1)	310(1)
PBESOL	428(2)	724(3)	195(4)	184(1)	246(1)	310(1)
RPBE	371(6)	679(3)	128(5)	169(1)	223(1)	271(1)

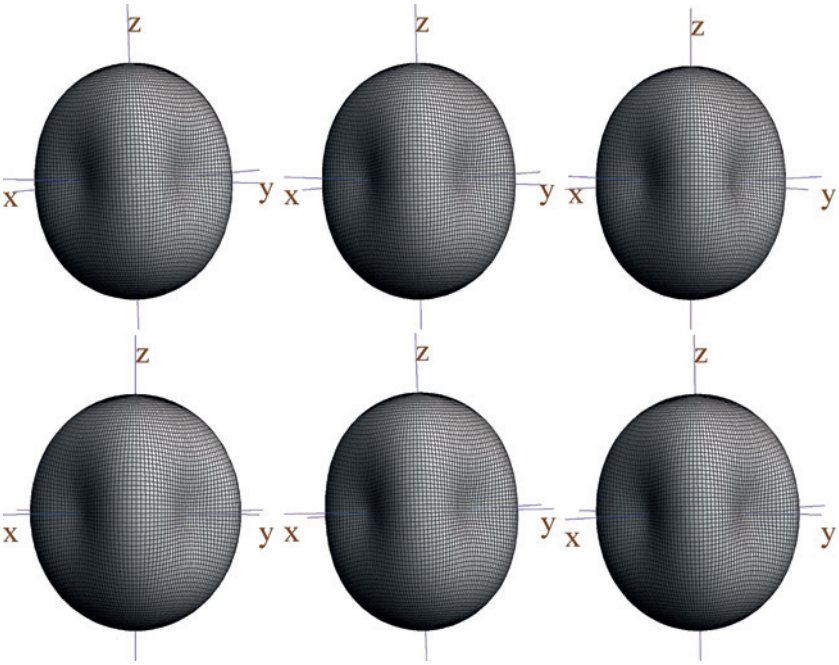

Fig. 2: Representation surfaces of the longitudinal elastic effect in stishovite. The top row are representation surfaces based on experimental data from Brazhkin et al. (2005), Weidner et al. (1982), and Yoneda et al. (2012), while the bottom row are results of model calculations based on the LDA, the GGA-PBE and the PBESOL *xc*-functional. In comparison to the experimental data, the LDA result is too isotropic, the PBE results too anisotropic while the PBESOL results are in good agreement with experiment.

The differences between the representation surfaces obtained from the experimental data are small, while it is clear that the LDA yields a too isotropic tensor, while the PBE exaggerates the anisotropy. The PBESOL results are intermediate and agree well with the experimental data sets.

In addition to often studied high symmetry crystals relevant to geophysics (see reviews by Karki et al. (2001) and Wentzcovitch et al. (2012b)) or materials science (e.g. TaC (Lopez-de-la Torre et al., 2005)), the reliability of the stress-strain approach has also been well established for low symmetry silicates (e.g. triclinic kyanite (Winkler et al., 2001)), organic crystals such as aspirin (Bauer et al., 2010), and inorganic compressible compounds such as thenardite (Arbeck et al., 2012).

As the predictive power of DFT calculations is independent of the applied stress (as long as e.g. an overlap of the core regions of the pseudoatoms in pseudopotential calculations is avoided) it is to be expected that the accuracy of the prediction of elastic stiffness coefficients at high pressures will be similar to those at ambient conditions. For high pressures, only few experimental data of low-symmetry compounds are available (Karki et al., 2001). Table 3 and Fig. 3 give a comparison of experimentally determined and computed elastic stiffness values of forsterite, Mg_2SiO_4 at 3.1 GPa and 16.2 GPa. The experimental data are from Zha et al. (1996).

Here, the results of the PBESOL calculation are in very good agreement at low pressure, and show a slight underestimation of the elastic tensor components with

Tab. 3: Experimentally determined (Zha et al., 1996) and computed elastic stiffness coefficients of forsterite, Mg_2SiO_4 at 3.1 GPa and 16.2 GPa.

	3.1 GPa		16.2 GPa	
	exp.	theo.	exp.	theo.
c_{11}	341.9 ± 7.5	334.7 ± 1.1	437.2 ± 5.9	416.1 ± 0.6
c_{22}	215.7 ± 2.3	209.3 ± 1.1	279.1 ± 5.9	269.8 ± 0.9
c_{33}	248.5 ± 4.9	241.0 ± 0.6	319.5 ± 4.0	301.0 ± 1.0
c_{44}	71.1 ± 0.8	71.6 ± 0.9	94.7 ± 1.3	89.0 ± 0.3
c_{55}	84.3 ± 0.8	83.1 ± 0.4	104.0 ± 1.2	96.3 ± 0.6
c_{66}	85.1 ± 0.7	84.4 ± 0.3	108.1 ± 1.3	102.8 ± 0.3
c_{12}	77.2 ± 2.8	77.3 ± 0.5	125.4 ± 4.5	122.2 ± 0.5
c_{13}	78.5 ± 2.1	78.2 ± 0.4	128.2 ± 2.6	123.1 ± 0.2
c_{23}	83.7 ± 2.5	79.2 ± 0.5	130.5 ± 2.3	124.4 ± 0.5

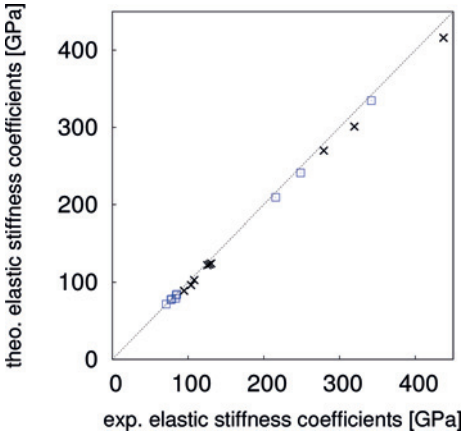

Fig. 3: Experimentally determined (Zha et al., 1996) and computed elastic stiffness coefficients of forsterite, Mg_2SiO_4 at 3.1 GPa (squares) and 16.2 GPa (crosses). The model calculations are based on the PBESOL *xc*-functional.

respect to the experimental data at higher pressures. However, the effort required for the experimental determination is significant, and increases dramatically for compounds of lower symmetry or at higher pressures, while the calculations take about two days on a small compute cluster.

For comparatively low pressures and a rather compressible compound, the reliability of the calculation of piezoelastic coefficients has been demonstrated by a comparison of experimental and theoretical data for thenardite, Na_2SO_4 (Arbeck et al., 2012). Here, it was found that for a low-symmetry compound with an experimentally determined bulk modulus of 38.2 GPa the piezoelastic coefficients were within 30% of the experimental values, but while the relative error is rather large, the absolute errors were always <6 GPa and, with two exceptions, smaller than 3 GPa.

Of geophysical interest is the thermoelasticity of mantle minerals. The state of the art of their computational determination has been recently reviewed by Wentzcovitch et al. (2010b) with an extensive comparison of experimental and theoretical studies. There are only few experimental data, but for example for MgO, the pressure and temperature derivatives of the elastic stiffness coefficients computed with the LDA+QHA are only in moderate agreement with experimental data.

2.4 Lattice dynamics

Phonon frequencies and the corresponding eigenvectors describing the displacement patterns for a specific mode can be obtained either by density functional perturbation theory (Baroni et al., 2001; Refson et al., 2006), which is also called "linear response" theory, or by a finite displacement approach, where the dynamical matrix is constructed by computation of forces acting on atoms when a specific atom is displaced. Both methods yield the same results. For example, in a theoretical study of the compression behavior of zoisite Winkler et al. (2008a) employed both a plane wave/pseudopotential linear response based calculation and a calculation where the valence electron wavefunction was expanded as a linear combination of localised pseudo-atomic orbitals and a finite displacement approach was employed for the phonon calculations. There was a very good agreement between the two approaches, independent of the pressure for which the structure and properties were calculated. The linear response approach allows one to compute LO/TO splitting. With DFT-based models, it is possible to compute frequencies and intensities of Raman (Porezag and Pederson, 1996; Milman et al., 2009), infrared (Porezag and Pederson, 1996; Refson et al., 2006), inelastic neutron scattering (Ryan et al., 2011) and inelastic X-ray scattering (Winkler et al., 2008b; Bosak et al., 2009) spectra. Commonly, the IR absorption spectrum of a powder is obtained from samples embedded in a matrix such as KBr. This can be included in the model (Balan et al., 2001).

An example where the pressure-induced intensity changes in Raman spectra was computed and compared to experiment is the study of ZrO_2 by Milman et al. (2009). In that study a pressure-induced transition into a fluorite-type cubic structure at 37 GPa was predicted, where the calculations indicated that the onset of the phase transition would manifest itself in a notable decrease in intensity and frequency of a Raman active mode. Up to 31 GPa, experimental data were available and the pressure-dependencies of the theoretical intensities are in good agreement with the corresponding experimental data (Milman et al., 2009).

If the phonon dispersion curves are known, it is possible to compute further properties, such as the heat capacity, Debye temperature, thermal diffuse scattering, or anisotropic displacement parameters. As the reliability with which these properties are computed is independent of an applied stress, DFT models can be used to predict these properties with the same accuracy as at ambient conditions. As has been mentioned above, the computation of phonon dispersion curves and of the phonon density of states is a prerequisite for the free energy calculations within the QHA. This then allows to introduce the effect of temperature into the calculations, albeit at a significant computational cost.

The accuracy of lattice dynamical properties depends on the level of theory employed, i.e. on the description chosen to represent exchange-correlation effects, in essentially the same way as ground state structures and elastic properties discussed above. More accurate hybrid functionals such as B3LYP can reduce the mean-square error of calculated phonon frequencies by a factor of two, as has been shown in the case of diopside (Prencipe et al., 2012). Unfortunately such efforts are often based on a rather empirical approach that modifies parameters of a hybrid functional to achieve good agreement with experiment (e.g., Többens and Kahlenberg (2011)).

3 Discussion and conclusion

In addition to the modeling studies of high pressure structures and their properties mentioned above, DFT based model calculations are extensively used to study

melting under high pressure (see review by Gillan et al. (2006)), and they are routinely employed for the prediction of novel high pressure phases (e.g. Pickard and Needs (2011), Lyakhov et al. (2013)). Several phases have been successfully predicted, but typically the predictions yield several polymorphs which are very close in energy and neglect the influence of temperature, which complicates comparisons with experiments. In experiments, on the other hand, it is often not even possible to index powder patterns unambiguously, as, for example in laser heated diamond anvil cell experiments the pattern of the new phase may overlap with the pattern of the pressure medium, of the thermal insulation and of the starting materials. The data evaluation becomes even more complicated if reactions instead of transitions between polymorphs are considered.

The rapid evolution of DFT-based model calculations will continue for some time. There are continuous ongoing developments to obtain improved exchange-correlation functionals and to extend the properties which can be computed. With respect to high pressure studies, this will be most relevant for structures and properties which depend on an accurate description of the *d*- and *f*-electrons and for those studies, where an accurate description of the band gap is required, such as in studies of pressure-induced metal-insulator transitions.

Other significant developments include more fundamental extensions, such as the development of time-dependent density functional theory (Gross et al., 1996), which will allow to model the response of structures to an extremely strong incident electromagnetic wave. Hence, it will be possible to model time resolved studies on the ps- and ns-time scale, such as are envisaged for experiments using X-ray free electron lasers.

One group of model calculations which currently pose a severe challenge are those calculations which address problems where the structure can only be represented by a very large super cell. These include statically or dynamically disordered materials, or defect structures, or studies aimed at understanding transport properties, e.g. across an interface in semiconductors. For such calculations the efficient parallelization of the computations is important. Currently most codes parallelize well for a few hundred to a few thousand cores, depending on the calculation and a comparison of several codes has shown that it is not straightforward to adopt the programs to very large computers (Plummer et al., 2006). It requires a significant effort to port these codes to new hardware with tens of thousands or possibly millions of cores (Jia et al., 2013), and this has not happened yet for the codes which are currently widely used.

In summary, DFT-based calculations are now an established tool for high pressure research, and ideally complement experimental approaches. A quantitative interpretation of spectra recorded at high pressures is generally possible, and the pressure-induced changes to structural parameters, the electron density, and physical properties can be obtained with a similar or higher accuracy than is possible by experiments. The main fundamental short-comings of the method are due to the difficulties in achieving a sufficiently accurate description of the exchange-correlation energy, and due to problems encountered when the supercell approach is providing an inadequate description of the real structure. The introduction of temperature is possible, but always increases the computational costs substantially.

Acknowledgement: We gratefully acknowledge financial support from the Deutsche Forschungsgemeinschaft (DFG), Germany, within SPP1236 (project Wi1232).

References

P. Hohenberg, W. Kohn, *Phy. Rev.* **1964**, *136*, B864.
W. Kohn, L. J. Sham, *Phys. Rev.* **1965**, *140*, A1133.
R. G. Parr, W. Yang, *Density-functional theory of atoms and molecules* (Oxford University Press, 1989).
E. S. Kryachko, E. V. Ludena, *Energy density functional theory of many-electron systems*, vol. 4 of *Understanding Chemical Reactivity* (Kluwer Academic Publishers, Dordrecht, 1990).
W. Koch, M. C. Holthausen, *A chemist's guide to density functional theory* (Wiley-VCH, 1999).
R. M. Martin, *Electronic structure* (Cambridge University Press, 2008).
E. Engel, R. M. Dreizler, *Density Functional Theory* (Springer, 2011), 531 pp.
J. Gale, A. Rohl, *Molecular Simulation* **2003**, *29*, 291.
X. Gonze, J. Beuken, R. Caracas, F. Detraux, M. Fuchs, G. Rignanese, L. Sindic, M. Verstraete, G. Zerah, F. Jollet, et al., *Computational Materials Science* **2002**, *25*, 478.
V. Milman, B. Winkler, J. White, C. Pickard, M. Payne, E. Akhmatskaya, R. Nobes, *International Journal of Quantum Chemistry* **2000**, *77*, 895.
M. Segall, P. Lindan, M. Probert, C. Pickard, P. Hasnip, S. Clark, M. Payne, *Journal of Physics: Condensed Matter* **2002**, *14*, 2717.
S. Clark, M. Segall, C. Pickard, P. Hasnip, M. Probert, K. Refson, M. Payne, *Zeitschrift für Kristallographie* **2005**, *220*, 567.
P. Giannozzi, S. Baroni, N. Bonini, M. Calandra, R. Car, C. Cavazzoni, D. Ceresoli, G. L. Chiarotti, M. Cococcioni, I. Dabo, et al., *Journal of Physics: Condensed Matter* **2009**, *21*, 395502.
G. Kresse, J. Furthmüller, *Phys. Rev. B* **1996**, *54*, 11169.
P. E. Blöchl, *Phys. Rev. B* **1994**, *50*, 17953.
G. B. Bachelet, D. R. Hamann, M. Schlüter, *Phys. Rev. B* **1982**, *26*, 4199.

D. Vanderbilt, *Phys. Rev. B* **1990**, *41*, 7892.
C. J. Pickard, R. J. Needs, *Journal of Physics: Condensed Matter* **2011**, *23*, 053201.
OPIUM, http://opium.sourceforge.net **2011**.
R. Dovesi, R. Orlando, B. Civalleri, C. Roetti, V. Saunders, C. Zicovich-Wilson, *Zeitschrift für Kristallographie* **2005**, *220*, 571.
B. Delley, *The Journal of Chemical Physics* **2000**, *113*, 7756.
V. Blum, R. Gehrke, F. Hanke, P. Havu, V. Havu, X. Ren, K. Reuter, M. Scheffler, *Computer Physics Communications* **2009**, *180*, 2175.
J. Soler, E. Artacho, J. Gale, A. Garcia, J. Junquera, P. Ordejon, D. Sanchez-Portal, *Journal of Physics: Condensed Matter* **2002**, *14*, 2745.
K. Schwarz, P. Blaha, G. Madsen, *Computer Physics Communications* **2002**, *147*, 71, Europhysics Conference on Computational Physics (CCP 2001), Aachen, Germany, Sep 05–08, 2001.
J. Perdew, K. Burke, M. Ernzerhof, *Phys. Rev. Lett.* **1996**, *77*, 3865.
B. Hammer, L. B. Hansen, and J. K. Nørskov, *Phys. Rev. B* **1999**, *59*, 7413.
J. P. Perdew, A. Ruzsinszky, G. I. Csonka, O. A. Vydrov, G. E. Scuseria, L. A. Constantin, X. Zhou, K. Burke, *Phys. Rev. Lett.* **2008**, *100*, 136406.
Z. Wu, R. Cohen, Physical Review B **2006**, *73*, 235116.
J. P. Perdew, K. Schmidt, *AIP Conference Proceedings* **2001**, *577*, 1.
J. Tao, J. P. Perdew, V. N. Staroverov, G. E. Scuseria, *Phys. Rev. Lett.* **2003**, *91*, 146401.
Y. Zhao, D. G. Truhlar, *The Journal of Chemical Physics* **2006**, *125*, 194101.
A. D. Becke, *The Journal of Chemical Physics* **1993**, *98*, 5648.
J. Heyd, G. E. Scuseria, M. Ernzerhof, *The Journal of Chemical Physics* **2003**, *118*, 8207.
J. Heyd, G. E. Scuseria, M. Ernzerhof, *The Journal of Chemical Physics* **2006**, *124*, 219906.
G. Ottonello, M. V. Zuccolini, B. Civalleri, *Calphad* **2009**, *33*, 457.
V. I. Anisimov, J. Zaanen, O. K. Andersen, *Phys. Rev. B* **1991**, *44*, 943.
S. L. Dudarev, G. A. Botton, S. Y. Savrasov, C. J. Humphreys, A. P. Sutton, *Phys. Rev. B* **1998**, *57*, 1505.
M. Cococcioni, S. de Gironcoli, *Phys. Rev. B* **2005**, *71*, 035105.
A. Seidl, A. Görling, P. Vogl, J. A. Majewski, M. Levy, *Phys. Rev. B* **1996**, *53*, 3764.
S. J. Clark, J. Robertson, *Phys. Rev. B* **2010**, *82*, 085208.
J. Perdew, A. Zunger, *Phys. Rev. B* **1981**, *23*, 5048.
S. Grimme, *Journal of Computational Chemistry* **2006**, *27*, 1787.
A. Grimme, J. Antony, S. Ehrlich, H. Krieg, *The Journal of Chemical Physics* **2010**, *132*, 154104.
P. Jurecka, J. Cerny, P. Hobza, D. R. Salahub, *Journal of Computational Chemistry* **2007**, *28*, 555.
M. J. Gillan, D. Alfe, J. Brodholt, L. Vocadlo, G. D. Price, *Reports of Progress in Physics* **2006**, *69*, 2365.
R. M. Wentzcovitch, Y. G. Yu, Z. Wu, in *Theoretical and computational methods in Mineral Physics: Geophysical applications*, edited by R. M. Wentzcovitch, L. Stixrude (Mineralogical Society of America, **2010a**), vol. 71 of *Reviews in Mineralogie & Geochemistry*, pp. 59–98.
R. M. Wentzcovitch, Z. Wu, P. Carrier, in *Theoretical and computational methods in Mineral Physics: Geophysical applications*, edited by R. M. Wentzcovitch and L. Stixrude (Mineralogical Society of America, **2010b**), vol. 71 of *Reviews in Mineralogie & Geochemistry*, pp. 99–128.
P. Söderlind, J. A. Moriarty, *Phys. Rev. B* **1998**, *57*, 10340.
W. B. Holzapfel, *Zeitschrift für Kristallographie* **2001**, *216*, 473.
A. Dewaele, P. Loubeyre, M. Mezouar, *Phys. Rev. B* **2004**, *70*, 094112.
A. Friedrich, E. A. Juarez-Arellano, E. Haussühl, R. Boehler, B. Winkler, L. Wiehl, W. Morgenroth, M. Burianek, M. Mühlberg, *Acta Crystallographica Section B* **2010**, *B66*, 323.
V. Milman, B. Winkler, *Zeitschrift für Kristallographie* **2001**, *216*, 99.
M. Alvaro, R. J. Angel, F. Camara, *American Mineralogist* **2012**, *97*, 11651176.
B. Winkler, J. D. Gale, K. Refson, D. J. Wilson, V. Milman, *Physics and Chemistry of Minerals* **2008a**, *35*, 25.
S. Baroni, P. Giannozzi, E. Isaev, in *Theoretical and computational methods in Mineral Physics: Geophysical applications*, edited by R. M. Wentzcovitch and L. Stixrude (Mineralogical Society of America, **2010**), vol. 71 of *Reviews in Mineralogie & Geochemistry*, pp. 39–57.
B. Winkler, M. T. Dove, *Physics and Chemistry of Minerals* **1992**, *18*, 407.
V. Milman, B. Winkler, M. I. J. Probert, *Journal of Physics: Condensed Matter* **2005**, *17*, 2233.
B. Winkler, M. Chall, C. J. Pickard, V. Milman, J. While, *Acta Crystallographica B* **2000**, *56*, 22.
L. Bayarjargal, L. Wiehl, A. Friedrich, B. Winkler, E. A. Juarez-Arellano, W. Morgenroth, E. Haussuehl, *Journal of Physics: Condensed Matter* **2012**, 24.
X. Li, R. Jeanloz, *Phys. Rev. B* **1987**, *36*, 474.
M. Chall, B. Winkler, P. Blaha, K. Schwarz, *Journal of Physical Chemistry* **2000**, *104*, 1191.
Y. G. Yu, V. L. Vinograd, B. Winkler, R. M. Wentzcovitch, *Physics of the Earth and Planetary Interiors* **2013**, *217*, 36.
S. Greenwald, *Nature* **1951**, *168*, 379.
J. Volger, *Nature* **1952**, *170*, 1027.
T. G. Worlton, R. M. Brugger, R. B. Bennion, *Journal of Physics and Chemistry of Solids* **1968**, *29*, 435.
G. Gorodetsky, R. M. Hornreich, S. Shtrikman, *Phys. Rev. Lett.* **1973**, *31*, 938.
L. Bayarjargal, B. Winkler, *Applied Physics Letters* **2013**.
P. Dera, B. Lavina, Y. Meng, P. V. B, J. *Solid State Chem.* **2011**, *184*, 3040.
S.-H. Shim, T. S. Duffy, R. Jeanloz, C.-S. Yoo, V. Iota, *Phys. Rev. B* **2004**, *69*, 144107.
A. Y. Dobin, W. Duan, R. M. Wentzcovitch, *Phys. Rev. B* **2000**, *62*, 11997.
C. Wessel, R. Dronskowski, *Journal of Solid State Chemistry* **2013**, *199*, 149.
B. B. Karki, L. Stixrude, R. M. Wentzcovitch, *Reviews of Geophysics* **2001**, *39*, 507.
W. Perger, J. Criswell, B. Civalleri, R. Dovesi, *Computer Physics Communications* **2009**, *180*, 1753.
R. Golesorkhtabar, P. Pavone, J. Spitaler, P. Puschnig, C. Draxl, *Computer Physics Communications* **2013**, *184*, 1861.
Accelrys, "Matrerials Studio" **2013**.
D. Arbeck, E. Haussühl, V. L. Vinograd, B. Winkler, N. Paulsen, S. Haussühl, V. Milman, J. D. Gale, *Zeitschrift für Kristallographie* **2012**, *227*, 503.
L. Lopez-de-la Torre, B. Winkler, J. Schreuer, K. Knorr, M. Avalos-Borja, *Solid State Communications* **2005**, *134*, 245.
B. Winkler, M. Hytha, M. C. Warren, V. Milman, J. D. Gale, J. Schreuer, *Zeitschrift für Kristallographie* **2001**, *216*, 67.

J. D. Bauer, E. Haussühl, B. Winkler, D. Arbeck, *Crystal Growth & Design* **2010**, *10*, 3132.
C. Zha, T. Duffy, R. Downs, H. Mao, R. Hemley, *Journal of Geophysical Research-Solid Earth* **1996**, *101*, 17535.
S. Baroni, S. de Gironcoli, A. Dal Corso, P. Giannozzi, *Reviews of Modern Physics* **2001**, *73*, 515.
K. Refson, P. Tulip, S. Clark, *Phys. Rev. B* **2006**, *73*, 155114.
D. Porezag and M. Pederson, *Phys. Rev. B* **1996**, *54*, 7830.
V. Milman, A. Perlov, K. Refson, S. J. Clark, J. Gavartin, B. Winkler, *Journal of Physics: Condensed Matter* **2009**, *21*, 485404.
K. R. Ryan, A. J. Ramirez-Cuesta, K. Refson, M. O. Jones, P. P. Edwards, W. I. F. David, *Phys. Chem. Chem. Phys.* **2011**, *13*, 12249.
B. Winkler, A. Friedrich, D. J. Wilson, E. Haussühl, M. Krisch, A. Bosak, K. Refson, V. Milman, *Phys. Rev. Lett.* **2008b**, *101*, 065501.
A. Bosak, I. Fischer, M. Krisch, V. Brazhkin, T. Dyuzheva, B. Winkler, D. Wilson, D. Weidner, K. Refson, V. Milman, *Geophysical Research Letters* **2009**, *36*, L19309.
E. Balan, A. M. Saitta, F. Mauri, G. Calas, *American Mineralogist* **2001**, *86*, 1321.
M. Prencipe, L. Mantovani, M. Tribaudino, D. Bersani, P. P. Lottici, *European Journal of Mineralogy* **2012**, *24*, 457.
D. M. Többens, V. Kahlenberg, *Vibrational Spectroscopy* **2011**, *56*, 265.
A. O. Lyakhov, A. R. Oganov, H. T. Stokes, Q. Zhu, *Computer Physics Communications* **2013**, *184*, 1172.
E. Gross, J. Dobson, M. Petersilka, in *Density Functional Theory II* **1996**, vol. 181 of *Topics in Current Chemistry*, pp. 81–172.
M. Plummer, J. Hein, M. F. Guest, K. J. D'Mellow, I. J. Bush, K. Refson, G. J. Pringle, L. Smith, A. Trew, *J. Mater. Chem.* **2006**, *16*, 1885.
W. Jia, Z. Cao, L. Wang, J. Fu, X. Chi, W. Gao, L.-W. Wang, *Computer Physics Communications* **2013**, *184*, 9.
W. H. Baur, A. A. Khan, *Acta Crystallographica Section B* **1971**, *27*, 2133.
D. Weidner, J. Bass, A. Ringwood, W. Sinclair, *Journal of Geophysical Research* **1982**, *87*, 4740.
V. Brazhkin, L. McNeil, M. Grimsditch, N. Bendeliani, T. Dyuzheva, L. Lityagina, *Journal of Physics: Condensed Matter* **2005**, *17*, 1869.
F. Jiang, G. D. Gwanmesia, D. T. I, D. T. S, *Physics of the Earth and Planetary Interiors* **2009**, *172*, 235.
A. Yoneda, T. Cooray, A. Shatskiy, *Physics of the Earth and Planetary Interiors* **2012**, *190*, 80.

Received April 25, 2013; accepted July 29, 2013
Published online January 9, 2014